ACS APPLIED MATERIALS & INTERFACES

Research Article

www.acsami.org

Self-Assembled Biodegradable Protein–Polymer Vesicle as a Tumor-Targeted Nanocarrier

Zhongyun Liu,[†] Chunhong Dong,[†] Xiaomin Wang,[†] Hanjie Wang,[†] Wei Li,[‡] Jian Tan,[‡] and Jin Chang*[,†]

[†]Institute of Nanobiotechnology, School of Materials Science and Engineering, Tianjin Key Laboratory of Composites and Functional Materials, Tianjin University, Tianjin 300072, P. R. China

[‡]Department of Nuclear Medicine, Tianjin Medical University General Hospital, Tianjin 300052, P. R. China

Supporting Information

ABSTRACT: Self-assembled nanostructures based on amphiphilic protein–polymer conjugates have shown great advantages in the field of nanomedicine such as inherent biocompatibility with biosystems because of their excellent performance. Herein, a novel biodegradable protein–polymer conjugate was prepared by covalently linking the tailor-made hydrophobic maleimide-functionalized poly(ε-caprolactone) (PCL) to hydrophilic bovine serum albumin (BSA) via the maleimide–sulfhydryl coupling reaction. This protein-based conjugate with a biodegradable polyester was reported for the first time, and the obtained biohybrid displayed well-defined structure, excellent biocompatibility and low cytotoxicity, and self-assembly behaviors similar to those of the traditional amphiphilic small molecules and block copolymers. The amphiphilic BSA–PCL conjugate can self-assemble into a nanosized vesicle with a negative surface charge. Furthermore, the self-assembled vesicle based on the BSA–PCL conjugate was functionalized via linking targeting ligand cetuximab to its surface to enhance cell uptake, and the doxorubicin (DOX)-encapsulated cetuximab-functionalized vesicle exhibited enhanced antitumor activity compared with that of free DOX *in vitro*. These results indicate that the biodegradable protein–polymer conjugate based on BSA and PCL had great potential as a drug delivery vehicle for cancer therapy.

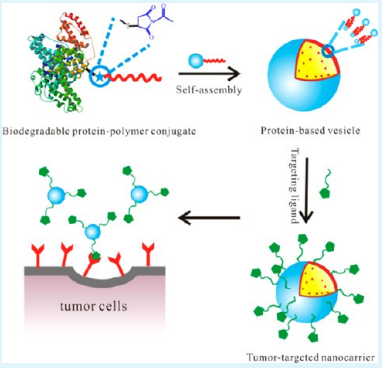

KEYWORDS: *protein–polymer conjugate, bovine serum albumin, poly(ε-caprolactone), self-assembly, nanocarrier*

1. INTRODUCTION

As a type of newly emerging biomaterial, the self-assembled nanostructures of biomolecules, especially the ones based on protein or DNA, are attracting more attention in the field of nanomedicine because of their precise geometry, versatile functions, and inherent biocompatibility with biosystems.[1−7] Inspired by the elegant functionalities of the biomolecules, a category of biohybrids, amphiphilic protein–polymer conjugates with a structure similar to that of a "tadpole" (hydrophilic protein as the head of the tadpole and hydrophobic polymer as its tail), has been designed. The tailor-made conjugates possess the advantages of both the protein and the polymer component, in which the protein element imparts biofunctional properties and the polymer component offers good stability, diversity, and some other fascinating properties.[8−11] Moreover, it has been established that the conjugates can self-assemble into nanosized aggregates with a wide range of morphologies such as micelles, micellar rods, and vesicles,[12−16] exhibiting structural characteristics and self-assembly behaviors similar to those of the traditional amphiphilic small molecules and block copolymers.

Until now, the existing research mainly focused on the synthesis of amphiphilic protein–polymer conjugates. The first example of amphiphilic protein–polymer conjugates was reproted by Nolte and co-workers, who attached a hydrophobic polystyrene (PS) chain to *Candida antarctica* lipase B (CALB) via the maleimide–sulfhydryl reaction.[17] The prepared CALB–PS conjugate exhibited amphiphilic properties similar to those of a small amphiphilic molecule and could self-assemble into bundles of fibers. Le Droumaguet and Velonia first reported the preparation of bovine serum albumin (BSA) [or human serum albumin (HAS)]–polystyrene (PS) giant amphiphiles via generating a PS chain directly from BSA or HAS *in situ*, and further research showed that multienzyme nanoreactors with high catalytic efficiency and permeability colud be built up by the self-assembly of the obtained giant amphiphile.[18] Recently, Ge, Zare, and their colleagues presented a new nanoparticle platform composed of a protein–polymer biohybrid amphiphile that was prepared by introduction of a hydrophobic polymethylmethacrylate (PMMA) chain onto a hydrophilic protein BSA via the "grafting from" approach.[19,20] Furthermore, camptothecin was encapsulated into the BSA–PMMA nanoparticles, and the nanoparticles showed great potential as drug delivery vehicles for cancer therapy. All these constructed amphiphilic protein–polymer conjugates mentioned above displayed great potential as nanocarriers and nanoreactors. In spite of the fruitful research conducted on the prepartion of amphiphilic protein–polymer conjugates, one of the most

Received: October 25, 2013
Accepted: January 23, 2014
Published: January 23, 2014

urgent requirements, however, is to design and construct a safe, biodegradable, and biocompatible amphiphilic protein−polymer conjugate that meets the criteria the conjugates have to fulfill as nanocarriers.[21] As a novel and expanding category of amphiphilic protein−polymer conjugates, the protein−polymer conjugates based on biodegradable polymers are supposed to be more ideal candidates for the materials of nanocarriers.[22−24] Regrettably, limited conjugates based on biodegradable polymers have been reported.

Herein, we describe a novel amphiphilic protein−biodegradable polymer conjugate consisting of bovine serum albumin (BSA) and poly(ε-caprolactone) (PCL). We chose BSA and PCL for the following reasons. BSA, a nutrient to cells, has been widely used as a drug or gene nanocarrier because of its numerous outstanding properties, for example, good biocompatibility, high degree of safety, excellent biodegradability, and facile functionalization.[25−28] PCL is also a biodegradable, biocompatible, and weakly toxic material approved by the U.S. Food and Drug Administration for medical applications. Biodegradable hydrophobic PCL imparted amphiphilic and self-assembly properties to the conjugate, and the BSA shell shielded the conjugate from potential immune responses and prevented the nanoparticles from undesired protein adsorption during the circulation in the blood due to the zwitterionic surface of BSA with abundant carboxyl and amino groups. The protein−polymer conjugate based on BSA and PCL displays great potential as a drug delivery vehicle. To the best of our konwledge, the BSA−PCL conjugate with a well-defined structure was first synthesized. Furthermore, we investigated the self-assembly behavior of the amphiphilic conjugate. The biodegradable protein-based vesicle was obtained via the self-assembly of the BSA−PCL conjugate and showed enhanced cell uptake by being decorated with cetuximab.

2. EXPERIMENTAL SECTION

2.1. Materials. Furan was obtained from Acros Organics and used without further purification. Bovine serum albumin (BSA, lyophilized powder, A3294) was purchased from Sigma-Aldrich and used with further reduced treatment via dithiothreitol (DTT). DTT was purchased from Sigma-Aldrich (St. Louis, MO). 5,5′-Dithiobis(2-nitrobenzoic acid) (DTNB, Ellman's reagent) and ε-caprolactone were obtained from Aldrich. All other reagent grade chemicals were obtained from local suppliers and used without further treatment.

2.2. Preparation of Furan-Protected Maleic Anhydride (C2). Furan-protected maleic anhydride was prepared using a previously reported method.[18] Briefly, 30.0 g of maleic anhydride (306 mmol) and 150 mL of toluene were added to a three-neck flask (500 mL) and stirred with a magnetic stir bar under a nitrogen atmosphere, and the reaction mixture was heated to 80 °C. Then 33.4 mL of furan (459 mmol) was solwly injected into the flask via syringe. After the mixture had been stirred for 6 h, the reaction was stopped and the mixture was cooled to ambient temperature. The white crystals were precipitated from the mixture after 1 h, collected via vacuum filtration, and washed with petroleum ether (3 × 30 mL). The resultant white powder was dried in a vacuum oven for 24 h, and the stucture of the compound was characterized by ^{1}H nuclear magnetic resonance (NMR) (Figure S1 of the Supporting Information).

2.3. Synthesis of Furan-Protected *N*-(2-Hydroxyethyl)-maleimide (C3). The furan-protected anhydride (15.05 g, 90.5 mmol) was suspended in 50 mL of methanol, and the mixture was cooled to 0 °C. Then 5.53 g of ethanolamine (90.5 mmol) dissolved in 30 mL of methanol was added dropwise to the flask, and the mixture was stirred for 5 min at 0 °C and 30 min at ambient temperature and finally refluxed with a reflux condenser at 80 °C. After 12 h, the reaction mixture was cooled to room temperature, and the reaction mixture was stored at 4 °C overnight. The product crystallized from the mixture and was collected via vacuum filtration. The crystals were dried in a vacuum oven for 24 h and then washed with methanol (3 × 20 mL). The compound was characterized by ^{1}H NMR (Figure S2 of the Supporting Information).

2.4. Synthesis of *N*-(2-Hydroxyethyl)maleimide (C4). Furan-protected *N*-(2-hydroxyethyl)maleimide (5.44 g, 26.0 mmol) and 50 mL of toluene were added to a three-neck flask under a nitrogen atmosphere. The reaction mixture was stirred and refluxed with a reflux condenser for 24 h. The reaction mixture was hot filtered, and the filtrate was stored at 4 °C overnight. The product crystallized from the mixture, was collected via vacuum filtration, and was dried under vacuum for 24 h.

2.5. Preparation of Maleimide-PCL. Maleimide-PCL was prepared via ring-opening polymerization (ROP) of CL using *N*-(2-hydroxyethyl)maleimide as an initiator and stannous octoate as a catalyst. Briefly, *N*-(2-hydroxyethyl)maleimide, CL, and a catalyst (0.5 wt % of the total reactants) were added to a Schlenk flask, and the reaction mixture was purged with argon for 30 min. Polymerization was conducted at 130 °C for 12 h under an argon atmosphere. Then the mixture was cooled to ambient temperature, and the obtained product was dissolved in dichloromethane and precipitated in cold diethyl ether. The precipitate was then collected via vacuum filtration, and the product was dried under vacuum for 24 h.

2.6. Reduction of BSA and Quantification of Free Thiols Using Ellman's Assay. BSA was reduced with dithiothreitol (DTT) as reported previously.[29] BSA was dissolved in phosphate-buffered saline [PBS, pH 8.3, 0.1 M, containing 1 mM ethylenediaminetetraacetic acid (EDTA)]. Dithiothreitol (DTT) was dissolved in PBS and then added dropwise to the BSA solution, and the mixture was stirred for 4 h. Then the solution was dialyzed using deionized water for 24 h [membrane molecular weight cutoff (MWCO) of 35000] and lyophilized to obtain reduced BSA.

Quantification of free thiols was performed via Ellman's assay as described previously.[29] 5,5′-Dithiobis(2-nitrobenzoic acid) (DTNB, Ellman's reagent, 4 mg) was dissolved in 0.1 M PB (1 mL, pH 6.8, containing 2 mM EDTA) to prepare the Ellman's reagent solution. A portion of the sample to be analyzed (5 mg) was added to buffer (2.50 mL) mixed with the Ellman's reagent solution (50 μL) and incubated for 45 min at ambient temperature. The absorbance (λ_{max} = 412 nm) of the 5-thio-2-nitrobenzoic acid (TNB) product was measured by UV−vis spectroscopy. The thiol content was obtained acrroding to the Beer−Lambert law. (The molar extinction coefficient of TNB was considered to be 14150 M^{-1} cm^{-1} at 412 nm.)

2.7. Conjugation of the Reduced BSA and Maleimide-PCL. The coupling of the maleimide-functionalized PCL to the reduced BSA was performed in a DMF/water mixture (10/90, v/v). The reaction was performed in a DMF/PBS mixture, and a DMF solution of maleimide-PCL (0.15 mM) was added to the reduced BSA in buffer (0.015 mM, 100 mM phosphate buffer, pH 6.8, 2 mM EDTA, 150 mM NaCl). The reaction was allowed to proceed overnight, and the excess reactant was removed by extensive dialysis against DMF and pure water for 48 h with a dialysis bag (MWCO of 35000). The powder of the BSA−PCL conjugate was obtained by a freeze-drying procedure.

2.8. Self-Assembly of BSA−PCL Conjugates. The aggregation of BSA−PCL conjugates was performed by the emulsion−solvent evaporation method described previously.[30] BSA−PCL conjugates (16 mg) were dissolved in 4 mL of dichloromethane at room temperature and sonicated with a bath sonicator for 5 min. During the ultrasonic treatment process, preformed organic solutions were added dropwise to 8 mL of deionized water. Dichloromethane was then removed using a rotary evaporator. The obtained solutions of the self-assembly of BSA−PCL conjugates were stored at 4 °C, and further characterization was conducted.

2.9. *In Vitro* Cytotoxicity. The MTT assay was used to assess the cytotoxicity of the BSA−PCL conjugate. In biref, U251 cells and MAD-MB-231 cells were seeded in 96-well microplates at a density of 5 × 10^3 cells/well and cultured with Dulbecco's modified Eagle's medium (DMEM, containing 10% fetal bovine serum, 1% penicillin, and 1% streptomycin) in the incubator under a 5% CO_2 atmosphere at

Scheme 1. Synthetic Procedure and Self-Assembly of the BSA−PCL Conjugates[a]

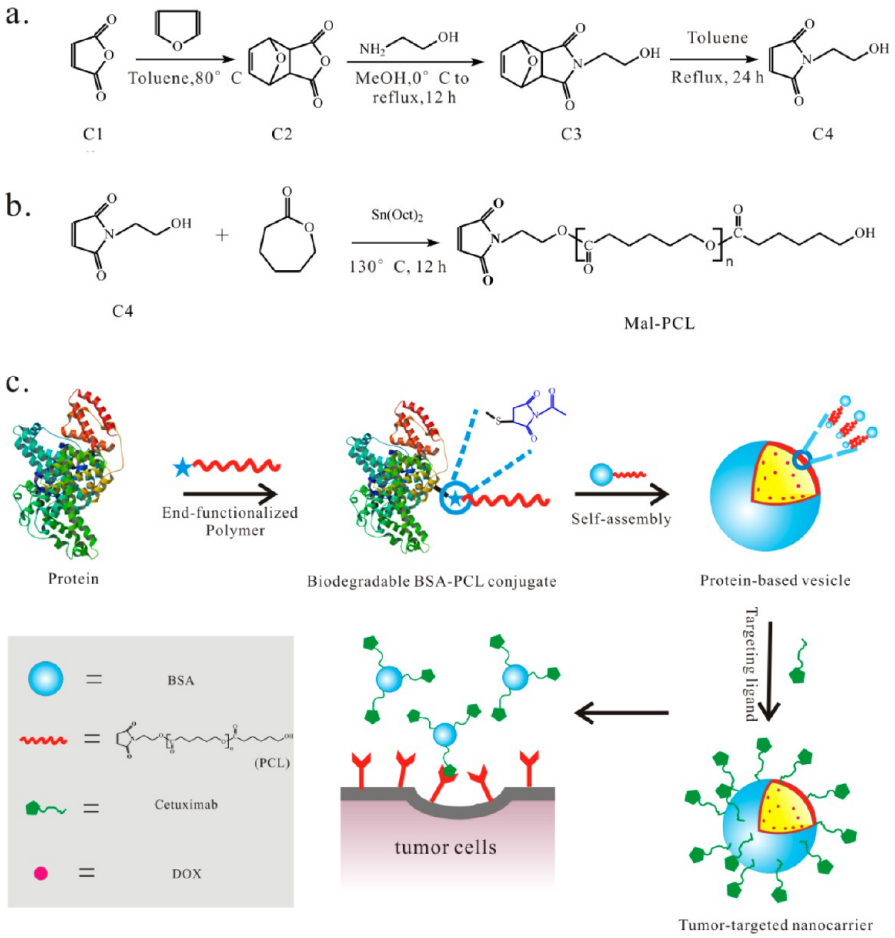

[a](a) Synthesis of *N*-(2-hydroxyethyl)maleimide. (b) Preparation of Mal-PCL via ROP of ε-caprolactone using *N*-(2-hydroxyethyl)maleimide as an initiator. (c) Covalent attachment of Mal-PCL to BSA via the maleimide−thiol reaction and the self-assembly of BSA−PCL conjugates and targeted modification with cetuximab.

37 °C for 24 h. Then, 100.0 μL of medium containing different BSA−PCL conjugate solutions was added to wells, and 100 μL of medium was added to wells containing control cells. The cells were further incubated for 24 h, and the MTT solution (5 mg/mL in water) was added to the wells (20 μL/well). After being incubated at 37 °C for 4 h, the medium was replaced with 200 μL of DMSO. The 96-well microplate was shaken with a shaking table for 10 min to dissolve the blue formazan precipitates, and the UV absorption of formazan at 570 nm was measured using a microplate reader. The cell survival rate was then calculated from the microplate reader of cells relative to that of nontreated cells.

2.10. Cellular Uptake of the BSA−PCL Vesicle. To investigate the cellular uptake of the protein-based vesicle formed from the BSA−PCL conjugate, we recorded fluorescence confocal microscopic images of the FITC-labeled vesicle in U251 cells and MAD-MB-231 cells. U251 cells and MAD-MB-231 cells were seeded into a small plate (1.0×10^5 cells/well). The cells were incubated in 3 mL of DMEM containing 10% FBS at 37 °C in the incubator for 24 h. Then 100.0 μL of medium containing the FITC-labeled vesicle and cetuximab-functionalized FITC-labeled vesicle solutions were added. After the cells had been incubated for 4 h, the medium was removed, and cells were washed three times with PBS. Then, the cells were observed by confocal laser scanning microscopy (CLSM) (Leica Microsystems GmbH, TCS SP 2).

2.11. Drug Loading and Releasing. To prepare the drug-loaded nanoparticles, doxorubicin was dissolved in the dichloromethane solution containing the BSA−PCL conjugates and treated with the same process of self-assembly of the BSA−PCL conjugate, and the powder of drug-encapsulated nanoparticles was obtained via a freeze-drying procedure.

A solution of the DOX-loaded BSA−PCL conjugate nanoparticles and free DOX were placed in cellulose ester membrane tubes (MWCO of 12000−14000), immersed in a PBS solution (pH 7.4), and shaken with a shaking table at 37 °C. The PBS was removed periodically (3 mL each time) to measure the UV absorbance using a UV−visible spectroscopy instrument (UV-2450, Shimadzu) at 480 nm, and 3 mL of fresh PBS was added to cellulose ester membrane tubes. The cumulative release was obtained according to the measured absorbance.

2.12. Cell Growth Inhibition Assay. In this experiment, U251 cells and MAD-MB-231 cells were seeded into 96-well microplates (5×10^3 cells/well). Cells were incubated for 24 h; various concentrations of free DOX and the DOX-encapsulated cetuximab-functionalized vesicle in fresh medium were added to the wells, and the cells were incubated for a further 48 h. Then the MTT solution (5 mg/mL in water) was added to the wells (20 μL/well) and incubated at 37 °C for 4 h. The medium was replaced with 200 μL of DMSO, and the 96-well microplates were shaken with a shaking table for 10 min to dissolve the blue formazan precipitates. The UV absorption of formazan at 570 nm was measured using a microplate reader. The cell survival rate was then calculated from the microplate reader of cells relative to that of nontreated cells

2.13. Characterization. ^{1}H NMR spectra of **C1**, **C2**, **C3**, **C4**, and Mal-PCL were obtained using a Varian Inova-500 MHz instrument (Varian Inc., Palo Alto, CA) with deuterated DMSO and $CDCl_3$ as solvents and TMS as an internal standard. The average molecular

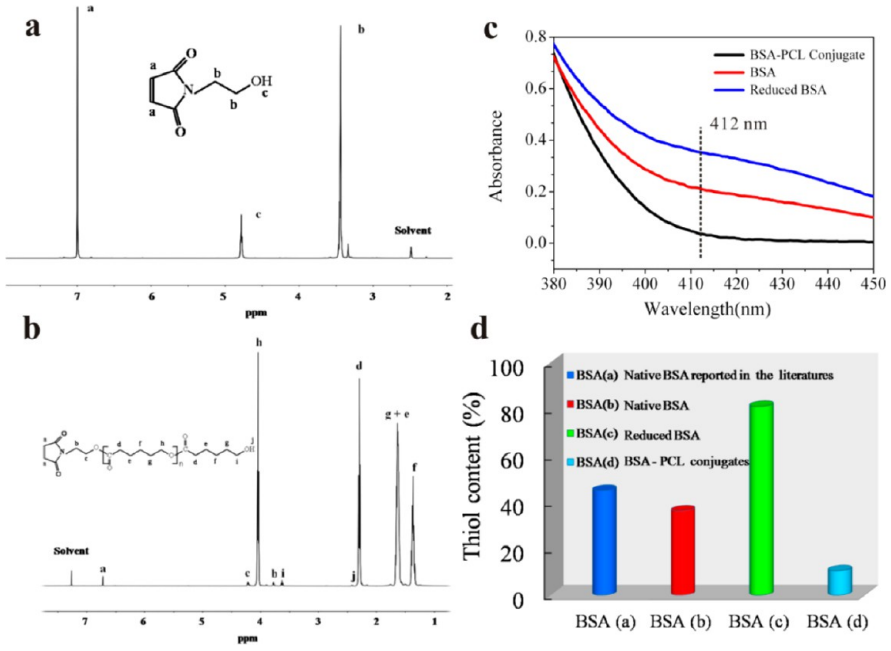

Figure 1. Characterization of the product. (a) ^{1}H NMR spectrum of the *N*-(2-hydroxyethyl)maleimide. (b) ^{1}H NMR spectrum of Mal-PCL. (c) UV spectra of the titrations performed with native BSA, reduced BSA, and the BSA−PCL conjugate using Ellman's reagent (DTNB). (d) Free thiol content of different samples: native BSA reported in previous studies [BSA(a)], native BSA used in our study [BSA(b)], reduced BSA with DTT [BSA(c)], and the BSA−PCL conjugate [BSA(d)].

weight of Mal-PCL and the polydispersity index (PDI) of the polymer were confirmed using a Waters 1515 gel permeation chromatograph (GPC, Waters Co.). Polystyrene standards with a narrow molecular weight distribution were used as calibration standards, and the elution phase was THF at a flow rate of 1.0 mL/min. Sodium dodecyl sulfate−polyacrylamide gel electrophoresis (SDS−PAGE) was conducted at 120 V using 1× Tris-glycine SDS (pH 8.3) as a running buffer and a polyacrylamide gel containing a 10% separating gel and a 5% stacking gel. The loading samples were prepared by mixing 7.5 μL of the measured solution (0.5 mg/mL) with 7.5 μL of loading buffer and then vortexed for a few seconds. The lanes were stained for protein using Coomassie Blue. Matrix-assisted laser desorption ionization time-of-flight mass spectroscopy (MALDI-TOF MS, Autoflex tof/tofIII, Bruker Daltonics Inc.) was employed to determine the molecular weights of BSA and the BSA−PCL conjugate with sinapinic acid as the matrix. BSA and conjugate solutions (1 mg/mL) were prepared by dissolving the sample in a mixture of acetonitrile and water (1/1, v/v) with 0.1% trifluoroacetic acid. The self-assembled morphology was observed by transmission electron microscopy (TEM). The measurement was performed on a JEOL-100CXII instrument in bright-field mode with an operating voltage of 100 kV. The solutions of self-assembled BSA−PCL conjugates (2.0 mg/mL) were dropped onto a carbon-coated copper grid and allowed to dry in air at room temperature and then negatively stained using 2% phosphotungstic acid. The size, PDI, and surface charge of the self-assemblies of BSA−PCL conjugates were determined by DLS using a Brookhaven Zetasizer (Brookhaven Instruments Ltd.) at 25 °C.

3. RESULTS AND DISCUSSION

3.1. Synthesis and Structural Characterization of the BSA−PCL Conjugate. In previous studies, two main ways to achieve the synthesis of amphiphilic protein−polymer bioconjugates have been reported.[11,31−36] One adopted approach is utilization of ε-amino groups of lysine residues on the protein via carbodiimide-mediated activated ester reactions or through Schiff base formation to form the protein−polymer conjugate. Another attachment method is the use of less abundant cysteine residues, instead of amino groups on the proteins. The former does not control the number of polymers conjugated and the conjugation site on the protein, while the latter based on thiol-ene chemistry such as maleimide-thiol reactions is of great interest beacuse the protein/polymer ratio and the conjugation site of the protein can be controlled precisely. Therefore, in this study, the latter approach was adopted to synthesize the well-defined BSA−PCL conjugate.

The strategy of the synthesis of the BSA−PCL conjugate is illustrated in Scheme 1. First, a tailor-made initiator, *N*-(2-hydroxyethyl)maleimide (**C4**), was synthesized, and maleimide-functionalized PCL (Mal-PCL) was prepared via ring opening polymerization (ROP) of CL with **C4** as the initiator and stannous octoate as the catalyst (Scheme 1a,b). The chemical structures of the intermediates (Figures S1 and S2 of the Supporting Information) and C4 and Mal-PCL (Figure 1a,b) were determined by ^{1}H NMR, and the molecular weight and PDI of the Mal-PCL were further measured via GPC (Figure S3 of the Supporting Information). Given that only ∼50% of the sulfhydryl group is available for conjugating polymers because of partial oxidation at Cys-34 of BSA,[11,29] BSA was reduced with dithiothreitol (DTT) to increase the number of available thiols before the next-step coupling reaction. Ellman's assay was used to confirm the average percentage of free thiols, and the result showed that it increased from approximately 45 to 95.3% after reduction (Figure 1c,d). This indicated approximately one thiol per BSA molecule could be used for polymer conjugation. Then BSA−PCL conjugates were prepared via maleimide−thiol reaction between Mal-PCL and reduced BSA. PCL was insoluble in an aqueous solution, and the coupling reaction was conducted in a carefully modulated DMF/PBS mixture. Ellman's assay indicated that the free sulfhydryl content was reduced to 15.8% after PCL had been covalently linked to BSA. According to Ellman's assay, there was still a small amount of residual BSA in the purified production, and it was difficult to remove it fully because of the

small difference in the molecular weight between native BSA and PCL-labeled BSA.

To verify PCL was attached to BSA, we determined the molecular weights of native BSA and the BSA–PCL conjugate by MALDI-TOF MS and SDS–PAGE. The molecular weight of native BSA was determined to be 66788 (Figure 2a), and the molecular weight of the BSA–PCL conjugate calculated via MALDI-TOF MS was 79914 (Figure 2b). Namely, the molecular weight of PCL attached to BSA was 13126, which was consistent with the GPC result for Mal-PCL and proved that the adopted attachment approach led to one conjugated polymer per protein. SDS–PAGE further verified these findings (Figure 2c). The electrophoretic band of native BSA was observed in lane 2, in accord with the position of the protein molecular weight marker at 66400 in lane 1. The electrophoresis band of the BSA–PCL conjugate (lane 3) revealed that PCL-labeled BSA had an electrophoretic mobility slower than that of native BSA, which suggested that the molecular weight of the BSA–PCL conjugate was larger than that of native BSA. Furthermore, the secondary structures of native BSA and the BSA–PCL conjugate were investigated via circular dichroism (CD), and the results show there was no significant change in the secondary structure after PCL conjugation and the α-helical structural element was predominant for both native BSA and the BSA–PCL conjugate.

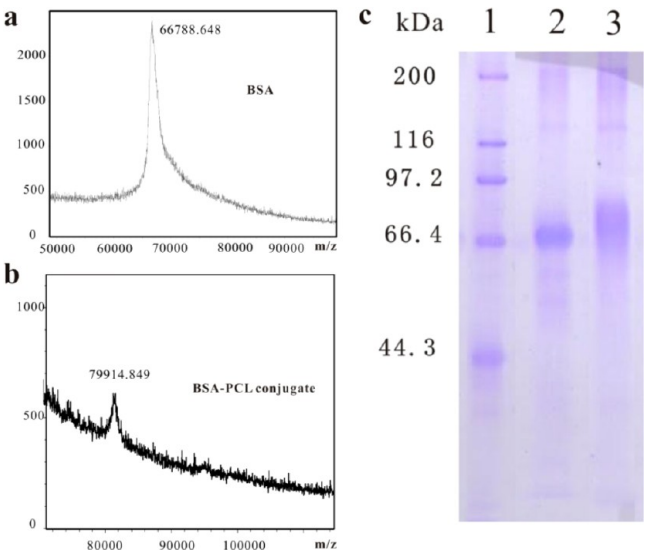

Figure 2. Characterization of the conjugate. (a) MALDI-TOF MS spectrum of native BSA. (b) MALDI-TOF MS spectrum of the BSA–PCL conjugate. (c) SDS–PAGE electropherogram of native BSA and the BSA–PCL conjugate.

3.2. Self-Assembly of the BSA–PCL Conjugate. The BSA-based conjugate decorated with hydrophobic polymer PCL was endowed with amphiphilic properties, and its self-assembly behavior was investigated. The self-assembly of the BSA–PCL conjugate was performed by the emulsion–solvent evaporation method, and a nanosized vesicle was obtained (TEM image shown in Figure 3a). The DLS measurement showed the average diameter was ~180 nm and the polydispersity index (PDI) was 0.164 (Figure 3b), in agreement with the TEM result. Furthermore, the BSA–PCL conjugate with lower-molecular weight PCL was prepared in a similar way, and its self-assembly behavior was also investigated (the MALDI-TOF MS and SDS–PAGE results in Figure S5 of the Supporting Information). The self-assembled morphology of the conjugate of BSA with lower-molecular weight PCL, by comparison, was a micelle (Figure 3c) instead of a vesicle, which may be due to the shorter length of the PCL chain. For the conjugates, as calculated via MALDI-TOF MS, the molecular weights of PCL and the BSA–PCL conjugates were 13126 and 4357, respectively. It has been proposed that

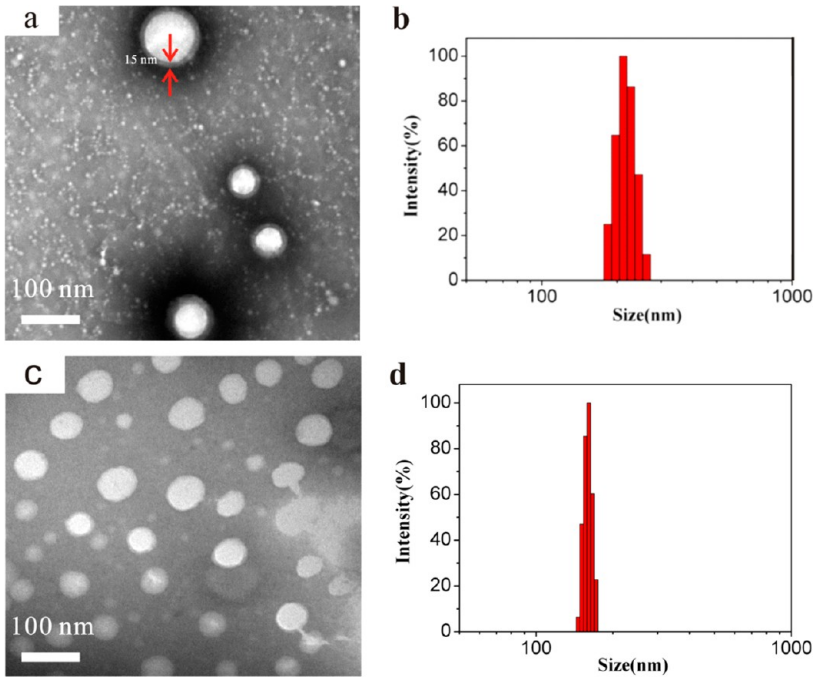

Figure 3. Different morphologies of the self-assembly of the BSA–PCL conjugate and histograms of the size distributions. (a and b) Vesicle and its size distribution. (c and d) Micelle and its size distribution.

dx.doi.org/10.1021/am404734c | ACS Appl. Mater. Interfaces 2014, 6, 2393–2400

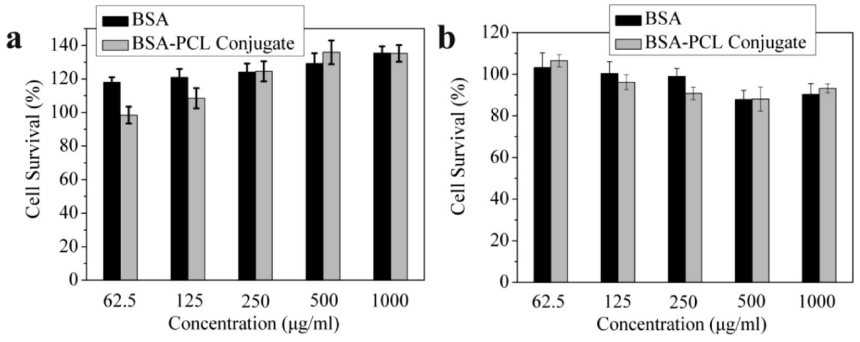

Figure 4. *In vitro* cytotoxicity of BSA and the BSA−PCL conjugate with U251 cells (a) and MAD-MB-231 cells (b) after incubation for 24 h. Error bars indicate the standard deviation of three separate experiments.

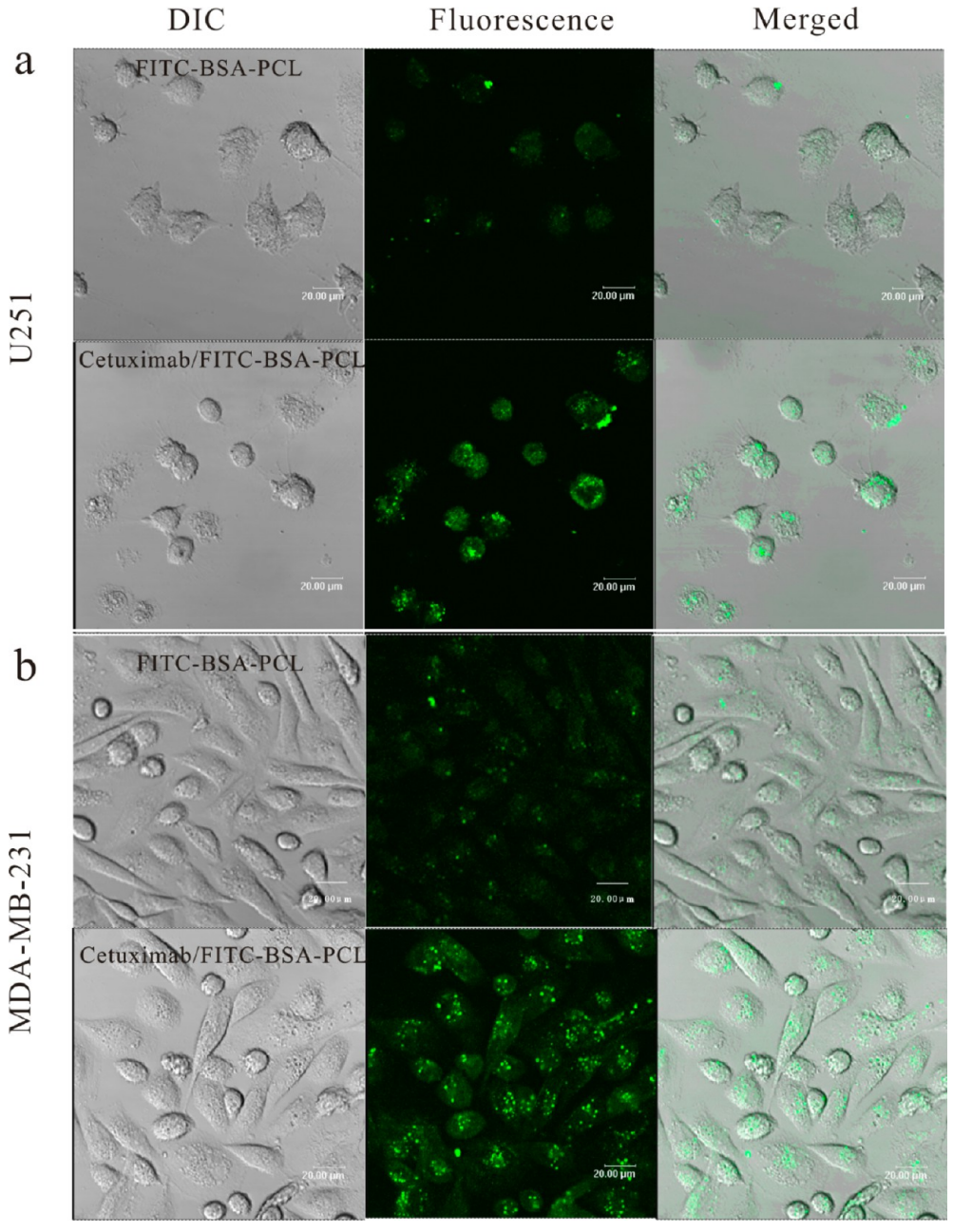

Figure 5. Confocal fluorescence images of U251 cells (a) and MDA-MB-231 cells (b) treated with the FITC-labeled BSA−PCL vesicle and cetuximab-modified FITC-labeled BSA−PCL vesicle for 4 h, respectively. The scale bars are 20 μm.

dx.doi.org/10.1021/am404734c | *ACS Appl. Mater. Interfaces* 2014, 6, 2393−2400

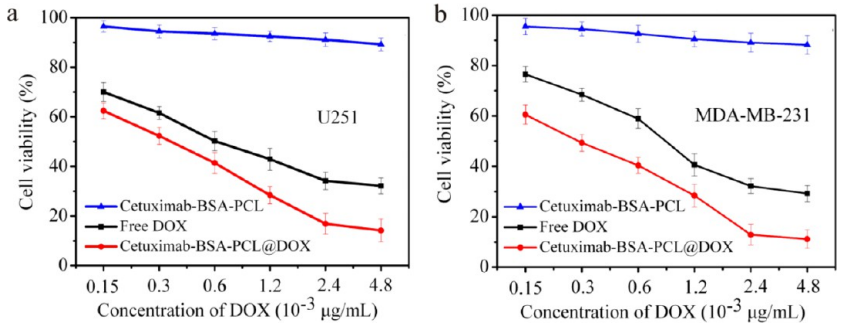

Figure 6. *In vitro* antitumor activity of two tumor cell lines treated with the DOX-encapsulated cetuximab-functionalized vesicle and free DOX: U251 cells (a) and MDA-MB-231 cells (b). Error bars indicate the standard deviation of three separate experiments.

amphiphilic polymers with the longer hydrophobic chains tend to form vesicles, and conversely, they favor micelle formation.[37−39] This result preliminarily indicated the self-assembled morphology of the BSA−PCL conjugate may be controlled by adjusting the length of PCL. More systematic studies are required to investigate the influence of the hydrophilic/hydrophobic ratio of the amphiphilic biohybrids on their self-assembled morphologies. The mean ζ potential of the obtained protein-based vesicle was also measured, and the value was −38.70 mV. The negative surface charge that resulted from the BSA shell could reduce undesired protein adsorption and provide good protection for the vesicle during the circulation in the body.

3.3. *In Vitro* Cytotoxicity and Cell Uptake of the BSA−PCL Conjugate. To test the cytotoxicity of the BSA−PCL conjugate, we assessed its cytotoxicity in two cell lines by the MTT assay: U251 cells and MAD-MB-231 cells. Figure 4 shows the cell viability with the different concentrations of the BSA−PCL conjugate and BSA after incubation for 24 h. No obvious cytotoxicity was observed for the BSA−PCL conjugate, and the viability of the BSA−PCL conjugate-treated U251 cells and MAD-MB-231 cells was almost around or even exceeded 100% over the whole concentration range. When the concentration of BSA and that of the conjugate were up to 1 mg/mL, ∼140% cell survival of the U251 cells was observed. The reason might be that BSA, which served as a nutrient for cells, could slightly promote the growth of cells. MTT results showed that the BSA−PCL conjugate had a low cytotoxicity for U251 cells and MAD-MB-231 cells.

To track the cell uptake of the protein-based vesicle formed from the BSA−PCL conjugate, the BSA−PCL conjugate was fluorescently labeled with FITC, which was covalently bound to the conjugate via the amine groups of the BSA, and the reaction was conducted in DMSO/$NaCO_3$-$NaHCO_3$ buffer (pH 9.4) mixtures. The cell uptake of the protein-based vesicle was investigated in two types of cells, U251 cells and MAD-MB-231 cells. To enhance the targeting ability of the protein-based vesicle against two types of cancer cells, cetuximab as a targeting ligand was linked to the periphery of the vesicle. As described above, after the cells had been treated with the vesicles (0.05 mg/mL) at 37 °C for 4 h, the medium was removed, and cells were washed three times with PBS and observed using confocal fluorescence microscopy. Figure 5 shows the fluorescent images of U251 cells and MAD-MB-231 cells incubated with the nontargeting vesicle and the modified vesicle. The images demonstrated that the cetuximab-functionalized vesicle was significantly internalized in the tumor cells, whereas the vesicle without cetuximab was weakly internalized. The active targeting of the modified vesicle was achieved by molecular recognition of the targeted cells via the ligand−receptor interactions [cetuximab can especially target the epidermal growth factor receptor (EGFR) on the surface of the cells]. For the vesicle without cetuximab, weak internalization was caused by the electrostatic repulsion between the vesicle and cell membrane with the same negative surface charge. The finding suggested that the protein-based vesicle could perform active targeting of U251 cells and MAD-MB-231 cells via cetuximab functionalization.

3.4. *In Vitro* Drug Release and Anticancer Activity of the BSA−PCL Vesicle. We investigated the *in vitro* antitumor activity of the cetuximab-functionalized vesicle as a nanodrug carrier. Doxorubicin (DOX) as a model drug for chemotherapy was loaded in the cetuximab-functionalized vesicle by self-assembly, and the encapsulation ratio of drug was measured to be ∼10 wt %. The drug release profile *in vitro* was obtained by adding a solution of free DOX and DOX-loaded cetuximab-functionalized vesicle to cellulose ester membrane tubes and placed in a PBS solution in a shaking water bath. The release studies showed that over the first period of 12 h, 32% of the loaded DOX was released from the DOX-loaded cetuximab-functionalized vesicle and no burst release was observed. Compared with the 54% release of free DOX, the drug-encapsulated vesicle exhibited a slow drug release behavior that could be attributed to the drug molecules being located in the interior of the vesicle. After 48 h, 93% of the DOX was released from free DOX while the amount of the drug-loaded vesicle released was only 55%. This slow release rate indicated the DOX-loaded cetuximab-functionalized vesicle had a good effect on the extended release *in vitro* (Figure S6 of the Supporting Information). Two cell lines, U251 cells and MDA-MB- 231 cells, were used to determine the inhibition of cell growth of the DOX-encapsulated vesicle, and the cell uptake in U251 cells was observed by a fluorescence microscope (Figure S7 of the Supporting Information). After the cells had been treated with the DOX-encapsulated vesicle and free DOX at different concentrations, the cell viability (antitumor activity of the vesicle and free drug) was determined by the MTT assay, and the results are shown in Figure 6. For the two tumor cell lines, the antitumor activity of the DOX-encapsulated cetuximab-functionalized vesicle and free DOX was increased with increasing amounts. The inhibition percentage of the DOX-encapsulated cetuximab-functionalized vesicle was >90%, whereas the value for free DOX was 70%. The free DOX exhibited a lower tumor inhibition rate than the DOX-encapsulated cetuximab-functionalized vesicle at the same concentration. The results confirmed that the DOX-encapsu-

lated cetuximab-functionalized vesicle had better therapeutic efficacy with respect to U251 cells and MDA-MB- 231 cells than free DOX.

4. CONCLUSIONS

In summary, we have developed a novel BSA−PCL conjugate with biodegradable PCL as the hydrophobic tail via thiol-ene chemistry. The obtained biohybrid displayed a well-defined structure, excellent biocompatibility, low cytotoxicity, and structural characteristics and self-assembly behaviors similar to those of the traditional amphiphilic small molecules and block copolymers. The protein-based vesicle with a nanosized scale and negative surface charge was formed by self-assembly of the BSA−PCL conjugate and suggested its potential use as a nanocarrier. Furthermore, the tumor-targeted ability of the protein-based vesicle is effectively enhanced via linking targeting ligand cetuximab, and the DOX-encapsulated cetuximab-functionalized vesicle showed enhanced antitumor activity compared with that of free DOX *in vitro*. The biodegradable amphiphilic BSA−PCL conjugate showed great potential as a nanocarrier.

■ ASSOCIATED CONTENT

Supporting Information

^{1}H NMR spectrum of 4,7,7a-tetrahydro-4,7-epoxyisobenzofuran-1,3-dione (**C2**) (Figure S1), ^{1}H NMR spectrum of 4,7-epoxyisobenzofuran-1,3-dione-4,7-epoxy-1*H*-isoindole-1,3(2*H*)-dione (**C3**) (Figure S2), gel permeation chromatography (GPC) profile of Mal-PCL (Figure S3), circular dichroism spectra of native BSA, reduced BSA, and the BSA−PCL conjugate (Figure S4), MALDI-TOF spectra and SDS−PAGE electropherogram of native BSA and the BSA−PCL conjugate (Figure S5), drug release behavior of the DOX-encapsulated cetuximab-functionalized vesicle and free DOX in a PBS solution (Figure S6), and characterization of Mal-PCL (Table S1). This material is available free of charge via the Internet at http://pubs.acs.org.

■ AUTHOR INFORMATION

Corresponding Author

*Telephone: +86-022-27401821. Fax: +86-022-27401821. E-mail: jinchang@tju.edu.cn.

Notes

The authors declare no competing financial interest.

■ ACKNOWLEDGMENTS

We gratefully acknowledge the National Natural Science Foundation of China (51373117 and 81070871), the Key Project of Tianjin Natural Science Foundation (13JCZDJC33200), the Tianjin research program of application foundation and advanced technology (12JCZDJC26000), and the Doctoral Base Foundation of the Educational Ministry of China.

■ REFERENCES

(1) Pàmies, P. *Nat. Mater.* **2013**, *12*, 778.
(2) Vendruscolo, M.; Dobson, C. M. *Nat. Chem. Biol.* **2013**, *9*, 216−217.
(3) Lai, Y.-T.; Tsai, K.-L.; Sawaya, M. R.; Asturias, F. J.; Yeates, T. O. *J. Am. Chem. Soc.* **2013**, *135*, 7738−7743.
(4) Simon, U. *Nat. Mater.* **2013**, *12*, 694−696.
(5) Yang, Y.; Zhao, Z.; Zhang, F.; Nangreave, J.; Liu, Y.; Yan, H. *Nano Lett.* **2013**, *13*, 1862−1866.
(6) Vial, S.; Nykypanchuk, D.; Yager, K. G.; Tkachenko, A. V.; Gang, O. *ACS Nano* **2013**, *7*, 5437−5445.
(7) Li, J.; Fan, C.; Pei, H.; Shi, J.; Huang, Q. *Adv. Mater.* **2013**, *25*, 4386−4396.
(8) Huang, X.; Li, M.; Green, D. C.; Williams, D. S.; Patil, A. J.; Mann, S. *Nat. Commun.* **2013**, *4*, 2239−2247.
(9) Reynhout, I. C.; Cornelissen, J. J.; Nolte, R. J. *Acc. Chem. Res.* **2009**, *42*, 681−692.
(10) Palivan, C. G.; Fischer-Onaca, O.; Delcea, M.; Itel, F.; Meier, W. *Chem. Soc. Rev.* **2012**, *41*, 2800−2823.
(11) De, P.; Li, M.; Gondi, S. R.; Sumerlin, B. S. *J. Am. Chem. Soc.* **2008**, *130*, 11288−11289.
(12) Thomas, C. S.; Xu, L.; Olsen, B. D. *Biomacromolecules* **2013**, *14*, 3064−3072.
(13) Thomas, C. S.; Xu, L.; Olsen, B. D. *Biomacromolecules* **2012**, *13*, 2781−2792.
(14) Thomas, C. S.; Glassman, M. J.; Olsen, B. D. *ACS Nano* **2011**, *5*, 5697−5707.
(15) Dirks, A. T. J.; Nolte, R. J.; Cornelissen, J. J. *Adv. Mater.* **2008**, *20*, 3953−3957.
(16) Kadir, M. A.; Lee, C.; Han, H. S.; Kim, B.-S.; Ha, E.-J.; Jeong, J.; Song, J. K.; Lee, S.-G.; An, S. S. A.; Paik, H.-j .*Polym. Chem.* **2013**, *4*, 2286−2292.
(17) Velonia, K.; Rowan, A. E.; Nolte, R. J. *J. Am. Chem. Soc.* **2002**, *124*, 4224−4225.
(18) Le Droumaguet, B.; Velonia, K. *Angew. Chem.* **2008**, *120*, 6359−6362.
(19) Ge, J.; Lei, J.; Zare, R. N. *Nano Lett.* **2011**, *11*, 2551−2554.
(20) Ge, J.; Neofytou, E.; Lei, J.; Beygui, R. E.; Zare, R. N. *Small* **2012**, *8*, 3573−3578.
(21) Couvreur, P. *Adv. Drug Delivery Rev.* **2013**, *65*, 21−23.
(22) Boyer, C.; Huang, X.; Whittaker, M. R.; Bulmus, V.; Davis, T. P. *Soft Matter* **2011**, *7*, 1599−1614.
(23) Alconcel, S. N.; Baas, A. S.; Maynard, H. D. *Polym. Chem.* **2011**, *2*, 1442−1448.
(24) Nicolas, J.; Mura, S.; Brambilla, D.; Mackiewicz, N.; Couvreur, P. *Chem. Soc. Rev.* **2013**, *42*, 1147−1235.
(25) Du, C.; Deng, D.; Shan, L.; Wan, S.; Cao, J.; Tian, J.; Achilefu, S.; Gu, Y. *Biomaterials* **2013**, *34*, 3087−3097.
(26) Han, J.; Wang, Q.; Zhang, Z.; Gong, T.; Sun, X. *Small* **2013**, DOI 10.1002/smll.201301-926.
(27) Zhang, Y.; Yue, X.; Kim, B.; Yao, S.; Bondar, M. V.; Belfield, K. D. *ACS Appl. Mater. Interfaces* **2013**, *5*, 8710−8717.
(28) Zhang, B.; Li, Q.; Yin, P.; Rui, Y.; Qiu, Y.; Wang, Y.; Shi, D. *ACS Appl. Mater. Interfaces* **2012**, *4*, 6479−6486.
(29) Heredia, K. L.; Bontempo, D.; Ly, T.; Byers, J. T.; Halstenberg, S.; Maynard, H. D. *J. Am. Chem. Soc.* **2005**, *127*, 16955−16960.
(30) Wang, H.; Zhao, P.; Liang, X.; Gong, X.; Song, T.; Niu, R.; Chang, J. *Biomaterials* **2010**, *31*, 4129−4138.
(31) Averick, S.; Simakova, A.; Park, S.; Konkolewicz, D.; Magenau, A. J.; Mehl, R. A.; Matyjaszewski, K. *ACS Macro Lett.* **2012**, *1*, 6−10.
(32) Sumerlin, B. S. *ACS Macro Lett.* **2012**, *1*, 141−145.
(33) Heredia, K. L.; Maynard, H. D. *Org. Biomol. Chem.* **2007**, *5*, 45−53.
(34) Jung, B.; Theato, P. *Adv. Polym. Sci.* **2013**, *253*, 37−70.
(35) Siegwart, D. J.; Oh, J. K.; Matyjaszewski, K. *Prog. Polym. Sci.* **2012**, *37*, 18−37.
(36) Canalle, L. A.; Löwik, D. W.; van Hest, J. C. *Chem. Soc. Rev.* **2010**, *39*, 329−353.
(37) Liu, G.-Y.; Chen, C.-J.; Ji, J. *Soft Matter* **2012**, *8*, 8811−8821.
(38) Du, J.; O'Reilly, R. K. *Soft Matter* **2009**, *5*, 3544−3561.
(39) Lee, J. S.; Feijen, J. *J. Controlled Release* **2012**, *161*, 473−483.